RESEARCH ARTICLE

Numerical Analysis of HBr-Cl2 Capacitive Coupled Plasma Using a Two-Dimensional Fluid Model

Iqra Shahzadi[1] **and Muhammad Waqar Ahmed**[1,*]

[1] Department of Physics, Riphah International University, Islamabad, Pakistan

Abstract

This research focuses on the computational analysis and numerical investigation of BrCl ion density within an HBr-Cl_2 capacitively coupled plasma system. A two-dimensional fluid simulation model was developed to examine the influence of varying the HBr: Cl_2 gas ratio on BrCl ion formation. The simulation framework incorporates fundamental plasma fluid equations, including the continuity equation, momentum conservation equations, and energy conservation equations, along with appropriate boundary conditions. The investigation specifically explored gas composition variations ranging from 10% Cl_2 and 90% HBr to 90% Cl_2 and 10% HBr, incremented in 20% steps. The radio frequency (RF) driving frequency was fixed at 13.56 MHz throughout the simulations. Results revealed a non-monotonic dependence of $BrCl^+$ ion density on the Cl_2 concentration; a mixture of 30% Cl_2 and 70% HBr yielded the highest $BrCl^+$ ion density, beyond which further increases in Cl_2 content suppressed $BrCl^+$ production due to depletion of the HBr precursor. Notably, elevated $BrCl^+$ ion densities were observed near the electrode edges and at the electrode center. The generated two-dimensional and three-dimensional simulation data offer foundational insights for practical industrial applications, particularly in advanced semiconductor etching and deposition technologies.

Keywords: two-dimensional fluid simulation, BrCl ion density, numerical analysis.

1 Introduction

In the semiconductor industry, plasma-based etching and deposition have become essential processes in microelectronic manufacturing, particularly through the use of halogen-based plasmas such as fluorine (F), chlorine (Cl), and bromine (Br). Compared to conventional wet chemical etching, dry etching is preferred due to its environmentally friendly nature and greater technical precision. Plasma etching offers numerous advantages over traditional methods, including enhanced anisotropy, better process control, and compatibility with advanced device geometries [1, 2]. The plasma chemistry within the reactor is further shaped by interactions with reactor walls, which can significantly alter the density of etch product species in halogen-based plasma environments [3]. Both bromine and chlorine based plasma have their own merits and limitations for dry etch plasma applications,

Submitted: 18 April 2025
Revised: 08 May 2025
Accepted: 09 May 2025
Published: 21 June 2025

Vol. 1, **No.** 1, 2025.
10.62762/JAM.2025.440251

***Corresponding author:**
✉ Muhammad Waqar Ahmed
waqarabbasi89@yahoo.com

Citation
Shahzadi, I., & Ahmed, M. W. (2025). Numerical Analysis of HBr-Cl2 Capacitive Coupled Plasma Using a Two-Dimensional Fluid Model. *ICCK Journal of Applied Mathematics*, 1(1), 15–24.

© 2025 by the Authors. Published by Institute of Central Computation and Knowledge. This is an open access article under the CC BY license (https://creativecommons.org/licenses/by/4.0/).

therefore it is necessary to discuss hidden aspects especially chemistry of bromine and chlorine based plasma [4]. The etching process strongly depends upon the type of gas especially type of halide gas used as the plasma generated species are important in dry etch applications. Many other parameters such as working pressure, gases flow rate, working temperature, type of plasma (RF, DC, Pulse DC or Microwave) strongly influence the etch process, like uniformity, proper selectivity, controlled etch rate and high performance of etching [5, 6]. The experimental process requires accurate and optimized parameters to achieve good results. In order to optimize correct parameters for the industrial application, numerical modeling and computational analysis of desired plasma is essential for defining the accurate parameters for performing experiments [7]. HBr-Cl_2 plasma is very useful in semiconductor industry especially for etching applications. In such plasma, the plasma chemistry is very important for etching applications therefore BrCl ions density is critical during the etching process in microelectronic manufacturing. After plasma confinement in capacitive coupled reactor, the BrCl ions formulates during some important chemical reactions like reaction of Cl radicals with HBr and reaction of bromine radicals with molecular chlorine, resulting in formation of BrCl and hydrogen and Cl. For these reactions electron impact ionization and ion impact dissociations both are responsible for the generation of BrCl ions. BrCl being polar diatomic molecule, with intermediate electronegativity difference makes it highly reactive [8, 10]. HBr has been widely adopted in polysilicon etching due to its favorable selectivity and passivation behavior [9]. The plasma chemistry of HBr/Cl_2 discharges, including species densities and reaction kinetics, has been investigated through self-consistent global models that account for electron impact reactions and ion flux composition [11]. BrCl ions play a vital role in etching, being volatile they can remove material without affecting the environment [13]. Precise control of plasma–surface interactions is especially critical in nanoscale ULSI device fabrication, where etch selectivity and feature integrity must be maintained at atomic scales [12]. Chlorine based plasmas have high etch rate as compared to bromine based plasma having less reactivity, but combination of BrCl can be dominant in etching process. Therefore composite of halide based plasma can be useful for etch applications [13]. The computational model designed in this research will be highly useful for determining the parameters for industrial applications.

2 Numerical Analysis

Fluid Simulation Model plays a vital role in this research. Different models and different numerical orders are used in this research to explain and evaluate fluid equations by different pattern of codes. Plasma is treated as a particular fluid in three-dimensional space, while species are influenced by the applied electric field. This model is based on density, flux, and mean energy of the species with respect to plasma. Equation is derivative of velocity distribution of Boltzmann equation. It offers us complete information comprising of all physical features like plasma chemistry, momentum, energy and electric field [14].

2.1 Reactor Geometry and Model

Our 2-Dimensional simulation comprised of geometry structure of CCP reactor which signify computational cell domain. The CCP reactor is operated by an RF power supply. CCP working principle is like a condenser in the circuit. It has two electrodes: one is grounded and the other is connected through the power supply. CCP reactor contains gas mixture as input via nozzle while output contained etched materials at bottom of reactor. The simulation domain is two-dimensional (R–Z cylindrical coordinates), with a radius of 15 cm and an electrode gap of 3 cm, discretized with equally spaced ΔR and ΔZ. The whole geometry is divided into a large number of grid cells. Each grid cell is filled with dielectric material at a specified voltage. For calculation of physical parameters such as density and electric field, the electrostatic field is calculated at each grid cell and the fluid equations are discretized at each cell and solved iteratively. Equation of continuity is used for calculation of energy and number of density and momentum. Electron density and potentials are calculated at center of cell and at grid points respectively. An advantage of this scheme is that plasma densities can be computed at the interface between the adjacent plasma and the dielectric surface. Boundary values of plasma densities are shifted to the half-grid points adjacent to the dielectric layer. Electrons are accelerated by the electric field, resulting in a large electron flux toward the reactor wall. It indicate that formation of negative potential via creation of sheath region. This sheath is comprised of positive charges which decelerated striking electrons and speed up ions to reactor up to equalization both electrons and ions. This neutrality of bulk plasma contained charges are attained via positive plasma potential which permits the ions to speed

up to reactor. Particles travels towards the reactor from higher density gradient towards lower density gradient. When energetic ions reach the substrate, they become implanted and sputter surface atoms into the gas phase. This model demonstrated that spatial variation happened in actual rate of discharge and as well as identification numerous species and reactions occurred in reactor. Figure 1 illustrates the schematic of proposed CCP reactor.

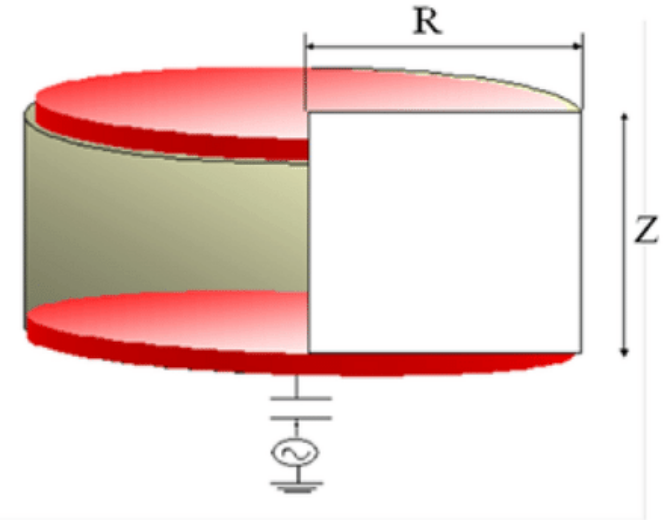

Figure 1. CCP Computational geometry.

2.2 Numerical model

A plasma numerical model is a computational tool used to simulate and study the behavior of plasma under various conditions. It employs mathematical equations and algorithms to capture the complex interactions and dynamics of plasma particles, electric fields, and chemical reactions, providing valuable insights into plasma processes. The following is the set of equations used in our model [14].

2.2.1 Equation of Continuity

Based on observation, one of the postulate the idea is that mass is neither created nor destroyed. In other words, it is conserved. This is termed the Principle of Conservation of Mass. This principle is applied to a fixed volume of arbitrary shape in space that contains fluid. This volume is called "Control Volume." Fluid is permitted to enter or leave the control volume.

Rate of increase of mass of material within the control volume = Net rate at which mass enters the control volume.

By equation of continuity

$$\frac{\partial n_e}{\partial t} + \nabla \cdot (n_e v) = 0 \tag{1}$$

where as

$$\frac{\partial n_e}{\partial t} = \text{Rate of change of number of density with time} + \nabla \cdot (n_e v) = \text{Divergence of } n_e \times v$$

Here $n_e = n_0 + n_1$ (n_1 is neglected because it is so small).

Assuming that density of electrons (n_e) is equal to density of ions (n_i), so

$$\frac{\partial n_1}{\partial t} + \nabla \cdot (n_0 v) = 0 \tag{2}$$

Differentiated with respect to t:

$$\frac{\partial^2 n_1}{\partial t^2} + n \cdot \nabla \frac{\partial v}{\partial t} = 0 \tag{3}$$

As we know from single fluid equation of plasma:

$$\frac{\partial v}{\partial t} = \frac{e}{m} \nabla \varphi \tag{4}$$

Substituting of equation (4) in (3):

$$\frac{\partial^2 n_1}{\partial t^2} + \frac{n_0 e}{m} \nabla^2 \varphi = 0 \tag{5}$$

$$\frac{\partial^2 n_1}{\partial t^2} + \left(\frac{n_0 e^2}{m \epsilon_0} \right) n_1 = 0 \tag{6}$$

2.2.2 Momentum Balance Equation

The Boltzmann equation is of fundamental importance in the kinetic theory of gases and plasmas. It expresses a mathematical description of the distribution function $f(r, v, t)$ of the particles at (r, v) in the phase space and at time t.

Boltzmann transformation equation is written as:

$$\frac{\partial f}{\partial t} + (\vec{v} \cdot \nabla) f + \frac{q}{m} (E + v \times B) \cdot \frac{\partial f}{\partial v} = \left(\frac{\partial f}{\partial t} \right)_c \tag{7}$$

Now multiplying the above equation with mv and integrate the entire equation with respect to velocity space:

$$\begin{aligned} m \int \vec{v} \frac{\partial f}{\partial t} d^3 v \nabla + m \int v (v \cdot \nabla) f d^3 v \\ + \frac{q}{m} \int v (E + v \times B) \cdot \frac{\partial f}{\partial v} d^3 v \\ = \int mv \left(\frac{df}{dt} \right)_c d^3 v \end{aligned} \tag{8}$$

Taking equation (8) and solving all terms individually.

Now take 1st term of equation (8) and solve it:

$$m\int \vec{v}\frac{\partial f}{\partial t}d^3v = m\frac{\partial}{\partial t}\int \vec{v}fd^3v \tag{9}$$

$$m\frac{\partial}{\partial t}\int \vec{v}fd^3v = m\frac{\partial}{\partial t}(n\vec{u}) \tag{10}$$

As knowing that

$$\int \vec{v}fd^3v = n\vec{u} \tag{11}$$

Now solve 2nd term of equation (8):

$$m\int \vec{v}(v\cdot\nabla)fd^3v = m\nabla\int \vec{v}\vec{v}fd^3v \tag{12}$$

$$m\nabla\int \vec{v}\vec{v}fd^3v = m\nabla\cdot(n\vec{v}\vec{v}) \tag{13}$$

$\vec{v}\vec{v}$ = velocity of particles which is equal to average and thermal velocity.

According to definition of velocity equation (13) will be convert as:

$$m\nabla\cdot(n\vec{u}\vec{u}) + \nabla(mn\vec{w}\vec{w}) \tag{14}$$

$$m\nabla\cdot(n\vec{u}\vec{u}) + \nabla p \tag{15}$$

$$m\left[u\nabla\cdot(nu) + n(u\cdot\nabla)u\right] \tag{16}$$

Now taking 3rd term of equation (8) evaluate it:

$$\begin{aligned}\int \frac{\partial}{\partial v}\cdot fv(E+v\times B)d^3v &= \int v(E+v\times B)\frac{\partial f}{\partial v}d^3v \\ &+ \int (E+v\times B)fd^3v \\ &+ \int vf\frac{\partial}{\partial v}\cdot(E+v\times B)d^3v\end{aligned} \tag{17}$$

Volume integral is converged into surface integral when $v=\infty$ & $f=0$. While 1st and 3rd term will be zero.

$$\begin{aligned}\oint_s^{v=0} fv(E+v\times B)d^3v &= \int v(E+V\times B)\frac{\partial f}{\partial v}d^3v \\ &+ \int (E+V\times B)fd^3v \\ &+ \int \frac{\partial}{\partial v}\cdot\varphi(vf)(E+v\times B)fd^3v\end{aligned} \tag{18}$$

As we have

$$\int v(E+v\times B)\partial f/\partial v d^3v = -\int (E+v\times B)fd^3v \tag{19}$$

$$-\int (E+v\times B)fd^3v = -n(E+v\times B) \tag{20}$$

From the result of equation (8) we get that:

$$\int mv\left(\frac{\partial f}{\partial t}\right)_c d^3v = P_{i,j} \tag{21}$$

Equation (21) is the representation of momentum change due to collision.

Whereas $P_{e,i}$ = change in momentum of electron due to ion, and $P_{i,e}$ = Change in momentum of ion due to electron.

Now putting the values of equations (10), (16), (20) & (21) in equation (8):

$$\begin{aligned}m\frac{\partial}{\partial t}(nu) + m\left[u\nabla\cdot(nu) + n(u\cdot\nabla)u\right] \\ +\nabla p - qn(E+v\times B) = P_{i,j}\end{aligned} \tag{22}$$

As from equation of continuity:

$$\frac{\partial n}{\partial t} + \nabla\cdot(nu) = 0 \tag{23}$$

$$\nabla\cdot(nu) = -\partial n/\partial t \tag{24}$$

Putting the values in equation (22):

$$\begin{aligned}mn\frac{\partial u}{\partial t} + mu\frac{\partial n}{\partial t} + m\left[-u\frac{\partial n}{\partial t} + n(u\cdot\nabla)u\right] \\ = nq(E+v\times B) - \nabla p + P_{i,j}\end{aligned} \tag{25}$$

$$mn\frac{\partial u}{\partial t} + mn(u\cdot\nabla)u = nq(E+v\times B) - \nabla p + P_{i,j} \tag{26}$$

$$mn\left[\frac{\partial u}{\partial t} + (u\cdot\nabla)u\right] = nq(E+v\times B) - \nabla p + p_{i,j} \tag{27}$$

Now represent equation (26) in the term of jth species:

$$\begin{aligned}m_j\frac{\partial}{\partial t}(n_ju_j) + \nabla\cdot(m_jn_ju_ju_j) \\ = eZ_jn_jE - \nabla P_j + m_jn_jv_ju_j\end{aligned} \tag{28}$$

$m_j\frac{\partial}{\partial t}(n_ju_j) + \nabla\cdot(m_jn_ju_ju_j)$ is the time-dependent momentum density representation equation while $eZ_jn_jE - \nabla P_j + mn_jv_ju_j$ is representation of forces

that are acting on the particles like pressure gradient, electric field and as well as particle collision.

Drift diffusion calculation of momentum equation assumed all the collisional process are dominant. Inertial effects of ions and time variation $\frac{\partial}{\partial t}(n_j u_j)$ are neglected. So if time is changing slowly then temperature will have time to equilibrate with their term of ideal gas equation.

$$\nabla P_j = \nabla n_j K_B T \tag{29}$$

Now putting the values of equation (29) in (28):

$$\begin{aligned} m_j \frac{\partial}{\partial t}(n_j u_j) + \nabla \cdot (m_j n_j u_j u_j) \\ = eZ_j n_j E - \nabla n_j K_B T + m n_j v_j u_j \end{aligned} \tag{30}$$

Neglecting inertial terms in equation (30) gives:

$$0 = eZ_j n_j E - \nabla n_j K_B T + m n_j v_j u_j \tag{31}$$

Now write in terms of mobility and diffusion coefficient:

$$\Gamma_j = q_j \mu_j n_j E - D_j \nabla n_j \tag{32}$$

2.2.3 *Energy Balance Equation*

It is clear that the continuity equation provides the value of electron/ion density at the grid points and the Poisson equation offers the value of potential and electric field at the grid points. These Poisson and Continuity equations work together giving numerical values.

Balance and constitutive equations for the material domain part of a plasma fluid model for tokamaks. These equations are derivative of the Boltzmann equation, by the application of the classical kinetic theory approach. They can also be calculated and demonstrated in Hamiltonian form with the help of material products (balance equations for a moving material domain). The entropy balance and the Gibbs-Duhem equations acceptable us to calculate the irreversible entropy production (source) term. All these entropy production and transport occurrences have been recognized respectively with a R-field and Stokes-Dirac interconnection structures.

Energy is not properly transmitted in electron-neutral collision because masses are differ in the collision. So Boltzmann EEDF approximation is used at constant momentum transfer frequency and constant kinetic pressure.

$$\Gamma_\epsilon = -\mu_\epsilon E_\epsilon - \frac{\partial}{\partial z}(D_\epsilon n_\epsilon) \tag{33}$$

where as

$$\mu_\epsilon = \frac{5}{3}\mu_e$$
$$D_\epsilon = \frac{5}{3}D_e$$

Putting these values in equation (33):

$$\Gamma_\epsilon = \frac{5}{3}\Gamma\epsilon_e + q \tag{34}$$

(D and μ = mean energy of electron and grad of mean energy)

Whereas Q = heat flux.

Heat flux is directly varied to gradient of mean energy. Electron of random motion is

$$\epsilon = \frac{3}{2}K_B T \tag{35}$$

and

$$q = -\frac{5}{3}D_e n_e \nabla\epsilon \tag{36}$$

Now substituting the value of q in equation (34):

$$\Gamma_\epsilon = \frac{5}{3}\epsilon\Gamma_e - \frac{5}{3}D_e n_e \nabla\epsilon \tag{37}$$

As we have

$$\Gamma_e = D_e \nabla n_e - \mu_e n_e E \tag{38}$$

Substituting equation (38) in the equation (37):

$$\Gamma\epsilon = \frac{5}{3}\epsilon\left(D_e \nabla n_e - \mu_e n_e E\right) - \frac{5}{3}D_e n_e \nabla\epsilon \tag{39}$$

$$\Gamma\epsilon = -\frac{5}{3}\epsilon\mu_e n_e E - \frac{5}{3}\epsilon D_e \nabla n_e - \frac{5}{3}D_e n_e \nabla\epsilon \tag{40}$$

$$\Gamma\epsilon = -\frac{5}{3}\epsilon\mu_e n_e E - \frac{5}{3}D_e \nabla\epsilon n_e \tag{41}$$

So

$$n_\epsilon = \epsilon n_e \tag{42}$$

Putting the values of equation (42) into (41):

$$\Gamma\epsilon = -\frac{5}{3}\mu_e n_\epsilon E - \frac{5}{3}D_e \nabla n\epsilon \tag{43}$$

As we know from equation of continuity:

$$\frac{\partial n_\epsilon}{\partial t} + \nabla \cdot \Gamma\epsilon = S\epsilon \tag{44}$$

$$S\epsilon = -e\Gamma\epsilon \cdot E - n_e \sum_r \epsilon_r n_r K_r \tag{45}$$

The above equation 1st term is representation of electron heat due to electric field and 2nd term is representative of collisional loss of electrons.

Whereas

1. n_r = Density of target particles i-e r
2. ϵ_r = Collision of type r

2.2.4 *Poisson's Equation*

Poisson's equation is one of the essential parts of Electrostatics, where we would solve the equation to calculate electric potential from charge distribution. In layman's terms, we can use Poisson's Equation to define the static electricity of an object.

The Poisson equation is precarious to attain a self-consistent solution in plasma fluid simulations used for Hall Effect thrusters and streamer discharges. The Poisson solution performs as source term of the unsteady nonlinear flow equations. At first step, solving the 2D Poisson equation with zero Dirichlet boundary conditions by a deep neural network is examined via multiple-scale architectures, defined in terms of number of branches, depth and receptive field.

Poisson equation is base for modelling of semiconductor devices and as well as used in reactor for calculation of self-consistent electric field.

Applying relation of Maxwell's equations:

$$\nabla \cdot D = \rho \tag{46}$$

where

$$D = \epsilon E \tag{47}$$

D = Electric field displacement

ϵ = permittivity tensor

Putting the value of D in equation (46):

$$\nabla \cdot \epsilon E = \rho \tag{48}$$

Also knowing that gradient vector for electric field is:

$$E = -\nabla \vec{v} \tag{49}$$

Substituting the value of E in equation (48):

$$\nabla \cdot (\epsilon \nabla \vec{v}) = -\rho \tag{50}$$

As

$$\rho = q_j n_j \tag{51}$$

So putting the value of equation (51) in equation (50):

$$\nabla \cdot (\epsilon \nabla \vec{v}) = -q_j n_j \tag{52}$$

2.2.5 *Boundary conditions*

At lower and upper boundary perpendicular position of electric field exist as zero and also at both boundaries upper and lower net flux also zero due to boundary conditions. At left boundary electric field is also zero. Plasma dielectric interface possessing two boundaries conditions i-e the dielectric surface where charge accumulates and boundary in front of dielectric layer.

Equations (7), (28), (35), and (52) are complemented by boundary conditions like as for electric potential at the electrodes and walls of reactor.

$$v_{rf} = v_0 \sin(2\pi f t) \tag{53}$$

where $v_0 = 300\,\mathrm{V}$ is the amplitude and the RF driving frequency is fixed at $f = 13.56\,\mathrm{MHz}$ throughout the simulations.

$V_{\text{ground}} = 0$ and $V_{\text{wall}} = 0$

Boundary conditions for fluxes of electrons and ions are being calculated as:

$$\Gamma_i = \text{sign}(q_i)\,\mu_i n_i E + \frac{1}{4} n_i v_{th,i} \tag{54}$$

where $v_{th,i} = \sqrt{8k_B T_i/(\pi m_i)}$ is the mean thermal velocity of charged species i.

For neutral species:

$$\Gamma_i^{in} = \frac{1}{4} n_i v_{th,j} \cdot \frac{\beta}{1 - \frac{\beta}{2}} \tag{55}$$

where β denotes the probability loss, equivalent to the sticking probability; γ denotes the sticking recombination probability of neutral species; and j represents the surface recombination rate of neutral species.

So

$$\Gamma_i^{out} = \sum_{j \neq i} \frac{\gamma_i}{\beta_j} \Gamma_j^{in} \tag{56}$$

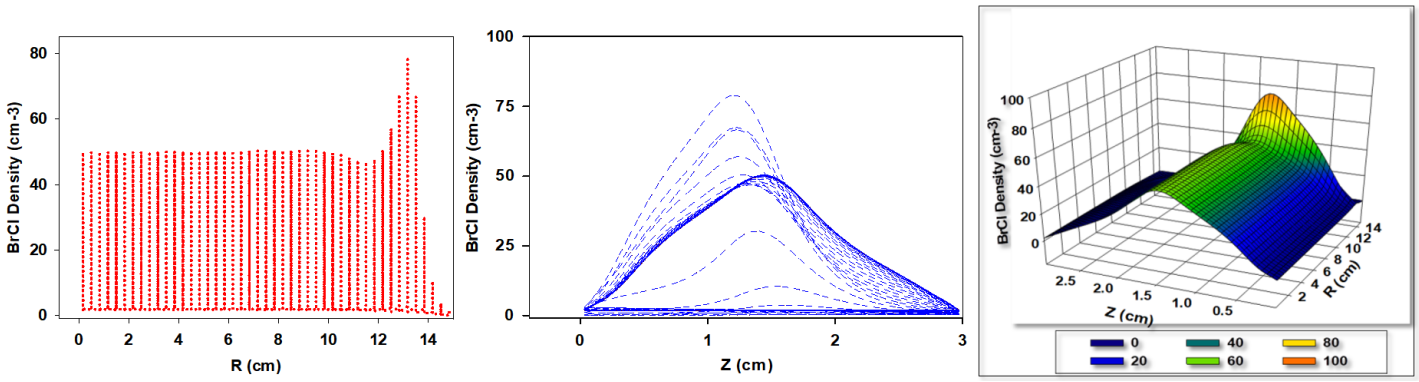

Figure 2. BrCl density for 10% Cl_2 and 90%HBr.

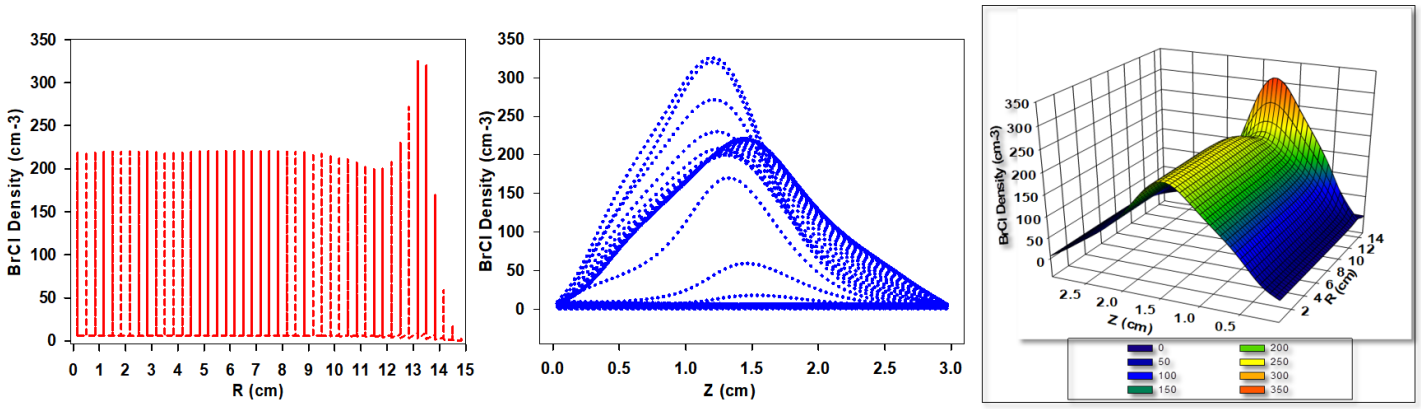

Figure 3. BrCl density for 30% Cl_2 and 70%HBr.

3 Chemical reactions

In the process of producing BrCl ions in an HBr/Cl_2 capacitive coupled plasma, several chemical reactions can occur. Here is a list of some possible reactions that could contribute to the formation of BrCl ions:

- HBr dissociation: $HBr \rightarrow H + Br$
- Cl_2 dissociation: $Cl_2 \rightarrow 2Cl$
- Cl excitation: $Cl \rightarrow Cl^*$ (excited state)
- Cl* + HBr reaction: $Cl^* + HBr \rightarrow H + BrCl$
- Br dissociation: $Br \rightarrow Br^*$ (excited state)
- Br* + Cl_2 reaction: $Br^* + Cl_2 \rightarrow BrCl + Cl$
- Br* + HBr reaction: $Br^* + HBr \rightarrow Br_2 + H$
- Br + Cl_2 reaction: $Br + Cl_2 \rightarrow BrCl + Cl$
- Br + HBr reaction: $Br + HBr \rightarrow Br_2 + H$

4 Results and Discussions

The fluid simulation of HBr - Cl_2 plasma was conducted to investigate the effect of varying gas ratios on BrCl ion density. This section presents the resulting trends in ion density and provides a detailed scientific explanation for the observed behavior and variations.

4.1 BrCl Ions Density for 10% Cl_2 and 90% HBr

Figure 2 illustrates the computationally derived spatial distribution of $BrCl^+$ ion densities for a gas mixture consisting of 10% Cl_2 and 90% HBr. Across the radial range from 0 to 11 cm, the $BrCl^+$ ion density remains relatively uniform. However, a slight decline is observed at 12 cm, followed by a sharp increase, reaching a maximum density of approximately 8.0×10^{10} cm^{-3} at a radial distance of 14 cm. Along the axial direction (z-axis) between the electrodes, the $BrCl^+$ ion density exhibits a bell-shaped profile, peaking at the midpoint between the electrodes. The data are visualized in a three-dimensional plot representing the initial $BrCl^+$ ion densities under the specified gas composition. This behavior results from a combination of physical and chemical phenomena, including gas-phase reactions, diffusion, transport mechanisms, electric field effects, and the influence of the plasma sheath, as well as electron and ion energy distributions. At the electrode edges, the elevated concentration of reactive species leads to increased $BrCl^+$ ion production. Additionally,

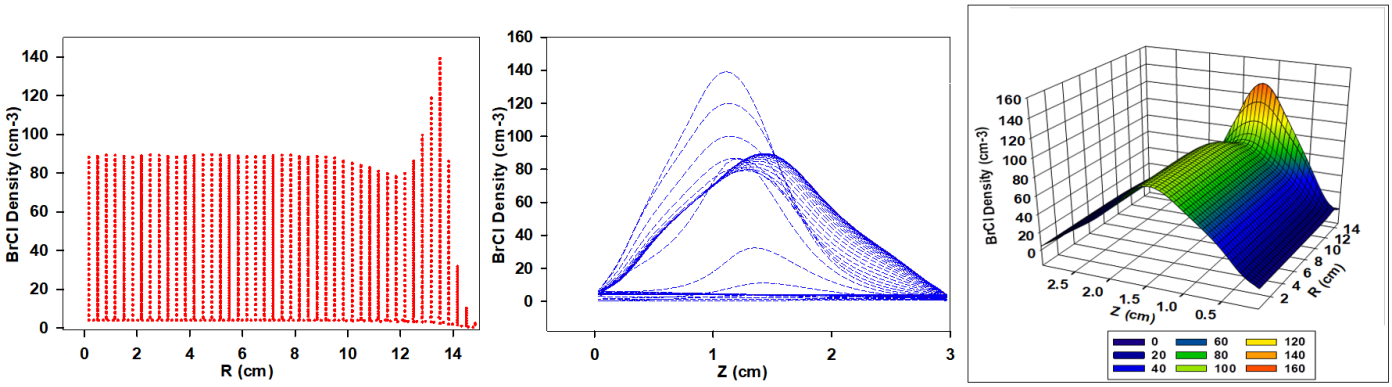

Figure 4. BrCl density for 50% Cl_2 and 50%HBr.

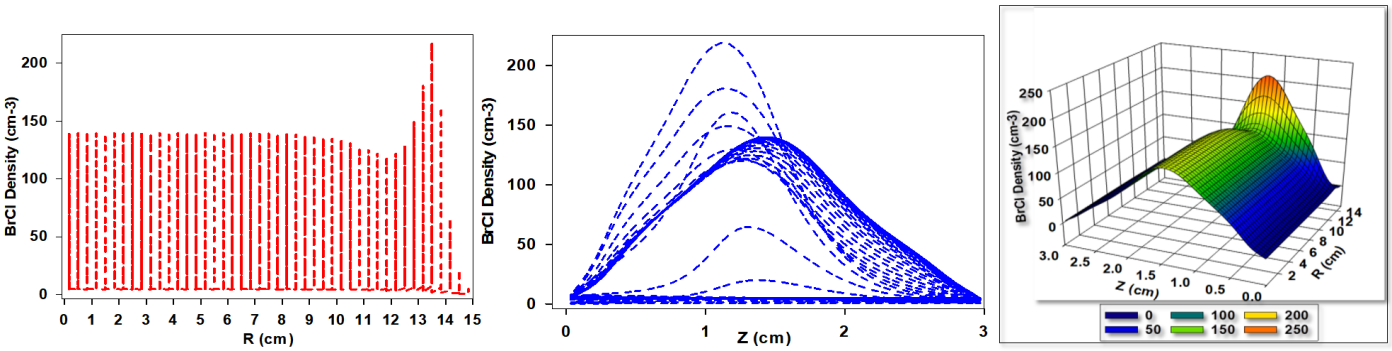

Figure 5. BrCl density for 70% Cl_2 and 30%HBr.

enhanced diffusion and transport fluxes at these edges further contribute to the localized density increase. The characteristics of the plasma sheath—acting as a transitional boundary between the plasma bulk and the electrode surface—also play a significant role, depending on operating parameters such as gas pressure, applied voltage, and the nature of chemical reactions. Regions with elevated electron and ion energies promote ionization processes, thereby increasing the $BrCl^+$ ion density.

4.2 BrCl Ions Density for 30% Cl_2 and 70% HBr

Figure 3 presents the simulated $BrCl^+$ ion density distribution for a gas mixture composed of 30% Cl_2 and 70% HBr. While the qualitative behavior of ion density variation remains consistent with previous observations, a significant quantitative increase in $BrCl^+$ ion density is evident. This enhancement is primarily attributed to the higher Cl_2 content, which intensifies chemical reaction rates, increases the dissociation of precursor molecules, and promotes overall ion generation. The elevated Cl_2 concentration facilitates more frequent and efficient reaction pathways, resulting in greater $BrCl^+$ ion production. The increased Cl_2 flux enhances both ionization and dissociation processes, thereby contributing to the elevated $BrCl^+$ ion density. Furthermore, the rise in chlorine content modifies

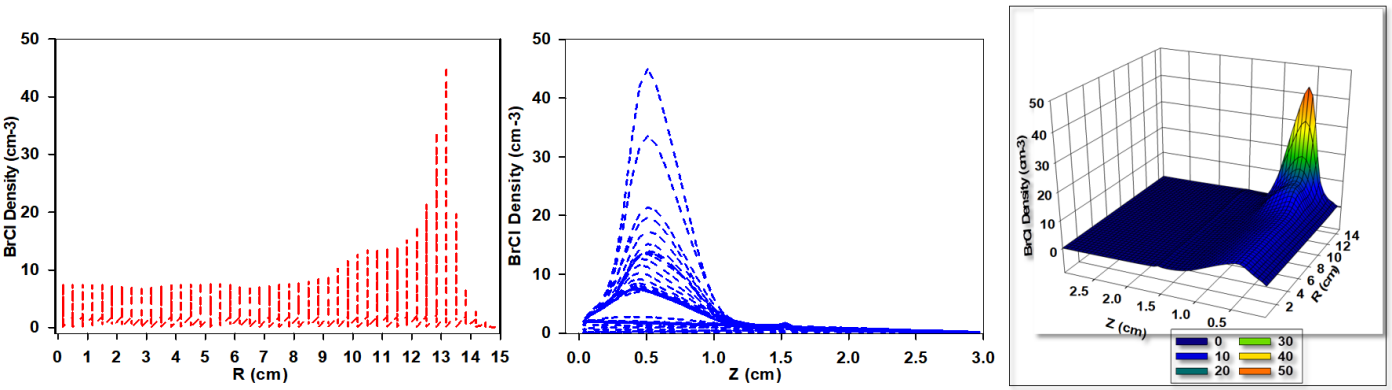

Figure 6. BrCl density for 90% Cl_2 and 10%HBr.

key plasma parameters such as electron temperature, electron density, and the spatial distribution of the electric field. These altered plasma characteristics further influence the formation and transport of $BrCl^+$ ions within the discharge region.

4.3 BrCl Ions Density for 50% Cl_2 and 50% HBr

Figure 4 illustrates computationally calculated BrCl ions density for 50:50 of Cl_2 and HBr respectively in CCP. This balanced ratio provided interesting results with similar shapes of density variations but differing in quantity. Many factors collectively influence the variations of BrCl ions density including optimized conditions for the formation of BrCl ions at balance gas ratios. This balanced ratio enhances collisional interactions between Cl_2-derived radicals and HBr, yet the overall $BrCl^+$ ion density is lower than that observed at the 30% Cl_2 ratio due to reduced HBr availability. At the balanced ratio, both ionization and transport processes also play an important role in the formation of BrCl ions.

4.4 BrCl Ions Density for 70% Cl_2 and 30% HBr

Figure 5 illustrates the variation in $BrCl^+$ ion density for a gas mixture containing 70% Cl_2 and 30% HBr, used in the simulation of a capacitively coupled plasma (CCP). While the overall trend in ion density behavior remains similar to previous cases, notable quantitative differences are observed. Specifically, the average $BrCl^+$ ion density in this mixture is lower than that in the 30% Cl_2 / 70% HBr case but slightly higher than the mixture with equal proportions of Cl_2 and HBr.

A slight shift in the bell-shaped profile of $BrCl^+$ ion density is evident, with peak densities now occurring closer to the electrode surfaces along the inter-electrode gap. The elevated Cl_2 ratio not only modifies the $BrCl^+$ ion density distribution but also increases the frequency of collisions and enhances ionization processes. This is primarily due to chlorine's lower ionization energy compared to HBr, which facilitates a higher rate of $BrCl^+$ ion generation. Despite these effects, the overall $BrCl^+$ ion density remains lower than that observed for the 30% Cl_2 and 70% HBr gas composition.

4.5 BrCl Ions Density for 90% Cl_2 and 10% HBr

Figure 6 illustrates that the simulation results reveal a significant reduction in $BrCl^+$ ion density at a gas composition of 90% Cl_2 and 10% HBr. Since HBr serves as a primary precursor in the formation of $BrCl^+$ ions, its low concentration leads to a substantial decline in ion generation. This pronounced imbalance in the Cl_2-to-HBr ratio disrupts the plasma chemistry, resulting in an excess of chlorine-containing species and an overall suppression of $BrCl^+$ ion production. Such a disproportionate gas mixture is unfavorable for applications that require stable or elevated $BrCl^+$ ion densities, particularly in industrial plasma processes. Additionally, this imbalance alters key plasma parameters, including the electric field distribution and the ionization dynamics, further contributing to the observed reduction in $BrCl^+$ ion density. Collectively, these factors explain the marked decrease in $BrCl^+$ formation under these conditions.

5 Conclusions

A dominant role of gas ratio on densities of BrCl ions has been observed. The balance and ideal gas ratio has been defined in this conclusion. The results found that a mixture of 30% Cl_2 and 70% HBr is ideal for the highest BrCl ions density at the electrode center. The findings confirm that a variety of physical and chemical processes, including ionization, dissociation, and diffusion—contribute to the generation of BrCl ions within HBr-Cl_2 capacitive coupled plasma. Also the spatial distribution of BrCl ion density is not solely dependent on gas composition; the position within the electrode region, particularly at the edges and the center, also has a pronounced impact. Under the current numerical modeling conditions, a mixture of 30% Cl_2 and 70% HBr was found to yield the highest BrCl ion density at the electrode center. The research provides baseline data for practical industrial applications.

Data Availability Statement

Data will be made available on request.

Funding

This work was supported without any funding.

Conflicts of Interest

The authors declare no conflicts of interest.

Ethical Approval and Consent to Participate

Not applicable.

References

[1] Flamm, D. L. (1990). Mechanisms of silicon etching in fluorine-and chlorine-containing plasmas. *Pure and Applied Chemistry, 62*(9), 1709-1720. [Crossref]

[2] Winters, H. F., & Coburn, J. W. (1992). Surface science aspects of etching reactions. *Surface Science Reports, 14*(4-6), 162-269. [Crossref]

[3] Cunge, G., Kogelschatz, M., & Sadeghi, N. (2004). Influence of reactor walls on plasma chemistry and on silicon etch product densities during silicon etching processes in halogen-based plasmas. *Plasma Sources Science and Technology*, 13(3), 522. [Crossref]

[4] Gul, B., & Rehman, A. U. (2016). Fluid Simulation of Capacitively Coupled HBr/Ar Plasma for Etching Applications. *Plasma Chemistry and Plasma Processing, 36*(5), 1363-1375. [Crossref]

[5] Li, C., Yang, Y., Qu, R., Cao, X., Liu, G., Jin, X., ... & Liu, Y. (2024). Recent Advances in Plasma Etching for Micro and Nano Fabrications of Silicon-based Materials: A Review. *Journal of Materials Chemistry C*. [Crossref]

[6] Donnelly, V. M., & Kornblit, A. (2013). Plasma etching: Yesterday, today, and tomorrow. *Journal of Vacuum Science & Technology A, 31*(5). [Crossref]

[7] Kushner, M. J. (2009). Hybrid modelling of low temperature plasmas for fundamental investigations and equipment design. *Journal of Physics D: Applied Physics, 42*(19), 194013. [Crossref]

[8] Efremov, A., Kim, Y., Lee, H. W., & Kwon, K. H. (2011). A comparative study of HBr-Ar and HBr-Cl 2 plasma chemistries for dry etch applications. *Plasma Chemistry and Plasma Processing, 31*, 259-271. [Crossref]

[9] Wagner, M. L., & Nine, R. (2013). The use of HBr in polysilicon etching. *Gases & Instrumentation International, 7*(4), 1-7. [Crossref]

[10] Cunge, G., Inglebert, R. L., Joubert, O., Vallier, L., & Sadeghi, N. (2002). Ion flux composition in HBr/Cl 2/O 2 and HBr/Cl 2/O 2/CF 4 chemistries during silicon etching in industrial high-density plasmas. *Journal of Vacuum Science & Technology B: Microelectronics and Nanometer Structures Processing, Measurement, and Phenomena, 20*(5), 2137-2148. [Crossref]

[11] Chung, S. Y., Yook, Y. G., Chang, W. S., Choi, H., Im, Y. H., & Kwon, D. C. (2024). Spatially averaged global model of HBr/Cl2 inductively coupled plasma discharges. *Physics of Plasmas, 31*(5). [Crossref]

[12] Ono, K., Ohta, H., & Eriguchi, K. (2010). Plasma–surface interactions for advanced plasma etching processes in nanoscale ULSI device fabrication: A numerical and experimental study. *Thin Solid Films, 518*(13), 3461-3468. [Crossref]

[13] Majeed, M., Gul, B., & Zia, G. (2020). Numerical investigation of the effect of variation of gas mixture ratio on density distribution of etchant species (Br, Br+, Cl, Cl+, and H) in HBr/Cl 2/Ar plasma discharge. *The European Physical Journal D, 74*, 1-10. [Crossref]

[14] Gul, B., Ahmad, I., & Zia, G. (2016). Numerical study of capacitive coupled HBr/Cl2 plasma discharge for dry etch applications. *Physics of Plasmas, 23*(9). [Crossref]

Dr. Muhammad Waqar Ahmed is an accomplished scientist in the field of low temperature plasma applications. Born on July 31st, 1980, in Pakistan, Dr. Ahmed obtained his Ph.D. from Jeju National University in South Korea in 2017. His doctoral research, conducted within the Department of Energy Systems and Chemical Engineering, focused on the fascinating realm of plasma physics. Following the successful completion of his Ph.D., Dr. Ahmed pursued further academic endeavors and undertook a Post-doctorate at Jeju National University from 2018 to 2019. During this period, he expanded his expertise in low temperature plasma applications, specializing in the sterilization applications of underwater plasma discharge. Dr. Ahmed's work encompassed both biological and industrial sectors, highlighting the broad range of potential applications for low temperature plasma. With an unwavering passion for scientific advancements, Dr. Muhammad Waqar Ahmed continues to explore and contribute to the field of low temperature plasma applications. His diverse research background and dedication to advancing plasma technology make him an invaluable asset to the scientific community.